nature communications

Article

https://doi.org/10.1038/s41467-025-60025-8

Electronic strong coupling modifies the ground-state intermolecular interactions in self-assembled chlorin molecules

Received: 20 September 2024

Accepted: 7 May 2025

Published online: 02 June 2025

Check for updates

Subha Biswas[1], Mainak Mondal[2,3], Gokul Chandrasekharan[1,3], Kavya S. Mony[1], Akshay Singh[2] ✉ & Anoop Thomas[1] ✉

The strong coupling of a molecular electronic transition with a quantized radiation field can result in modified photophysics compared to its uncoupled counterparts. Often, such changes are attributed to kinetic factors, overlooking the possible modifications to intermolecular interactions. The spin-cast films of chlorin e6 trimethyl ester (Ce6T) show an excitonic coupling band in absorption resulting from their ground-state intermolecular interactions and subsequent excimer-like emission upon photoexcitation. Interestingly, the electronic strong coupling (ESC) of the Ce6T Soret and Q-band suppresses the intermolecular excitonic interactions that otherwise exist in the Ce6T thin films and brings back the monomer-like emission characteristics. Our experiment provides a unique tool to tune the molecular assembly without involving chemical modifications. Our results suggest that ESC can induce modification to the intermolecular interaction forces that hold together the molecular assemblies in the ground state, which is a significant step toward understanding the fundamentals of polaritonic chemistry in detail.

Like the zero-point energy of a molecular vibrational mode, the electromagnetic field also has quantum (vacuum) fluctuations for its lowest state[1]. Interestingly, the ubiquitous phenomenon of spontaneous emission results from the interaction of matter with the electromagnetic vacuum states[2]. Since there can be an infinity of vacuum states in a medium in a given frequency interval, one may overlook the interaction of the former with the matter[1]. A Fabry-Perot cavity, for instance, can confine the photons within the field boundary conditions, changing the availability and enhancing the amplitude of radiation modes[3–5]. The molecules inside such cavities can interact collectively with the resonant cavity mode, resulting in a weak or strong light-matter coupling regime[3–9]. The weak coupling modifies emission intensities and decay rates and is known as the Purcell effect[10] or sometimes as metal-enhanced emission[11,12]. The cavity and matter exchange energy faster than dissipation in the strong coupling regime, forming new hybrid light-matter states called the polaritonic states[3–5]. The half-light, half-matter characteristic of the polaritonic state renders unique properties to the system compared to their uncoupled counterparts[3–9]. Besides the Fabry-Perot cavity, numerous other architectures, such as plasmonic substrates, hole arrays, Bloch surface waves, whispering gallery mode resonators, and dielectric metasurfaces, can confine electromagnetic radiation and achieve strong coupling[6–8].

The collective electronic strong coupling (ESC), wherein the electronic transition dipoles hybridize with the cavity modes, has been achieved in many excitonic systems such as J-aggregates, quantum wells, small organic dyes, and polymers[6–8]. It has resulted in modifying many photo-induced processes such as photoisomerization[13–16], energy transfer[17–20], and photobleaching[21,22]. Only a few experiments[23,24] and theoretical studies[25–27] examined the effect of ESC on the ground-state molecular properties, such as work function[23] and free energy[24,26]. While most of the reports on molecular photophysics under ESC focused on kinetics, the impact of ESC on molecular interaction and assembly is unexplored. On the other hand, multiple

[1]Department of Inorganic and Physical Chemistry, Indian Institute of Science, Bengaluru 560012, India. [2]Department of Physics, Indian Institute of Science, Bengaluru 560012, India. [3]These authors contributed equally: Mainak Mondal, Gokul Chandrasekharan. ✉e-mail: aksy@iisc.ac.in; athomas@iisc.ac.in

experiments have shown that collective vibrational strong coupling (VSC) leads to changes in ground-state intermolecular interactions[28–33]. Here we use chlorin e6 trimethyl ester (Ce6T) as an example to investigate the role of ESC on molecular self-assembly and to identify if there are parallels between ESC and VSC. Our results show the surprising observation that the ESC of the Q- and the Soret band of the Ce6T alter the ground-state intermolecular interactions that otherwise exist in films of Ce6T, providing completely different photophysical properties to the Ce6T.

Results

Excimer-like emission from Ce6T in thin films

The molecule Ce6T (structure schematically shown in Fig. 1A), which is a derivative of *chlorophyll-a*[34], is less likely to form complete H- or J-aggregates without the metal center[35]. Electronic strong coupling experiments typically require an absorbance of ca. 0.2 or higher for the active material to facilitate the effective energy exchange[4]. Therefore, ESC experiments often use a high molecular concentration to obtain the required optical density, because the cavity path length must be within a few hundred nm for effective field confinement. Accordingly, we prepared a Ce6T film (16 wt%; 400 nm thickness) in a polystyrene (PS) matrix by spin-coating the solution of Ce6T and PS in toluene. The absorption spectrum of the non-cavity Ce6T film (Fig. 1B, solid curve) retains the spectral features and the intensity ratio of the Soret (405 nm) and Q-band (668 nm) as in the solution (Fig. 1B, dotted curve). It indicates the absence of an extended J-aggregate, as seen in metal coordinated chlorin, where both the Soret and Q-band absorbance reduce significantly with the simultaneous formation of the intense redshifted J-aggregate band[35,36]. Interestingly, we notice a new absorption band in the thin film, peaking at 727 nm. The band is observable when the Ce6T amount is above one wt%, and its intensity grows slightly upon increasing the concentration with a concomitant redshift (Supplementary Fig. 1A, B), suggesting a coupling and delocalization of the transition dipole[37–39]. The appearance of the new band indicates that spin coating leads to the preorganization and assembly[40] of the molecules in the films, albeit the metal center is absent. We verified that the Ce6T assembly is not just due to the PS matrix by preparing films in a non-aromatic polymer, poly(methyl methacrylate) (Supplementary Fig. 2). Thus, the absorption band at 727 nm is due to the ground-state intermolecular interaction of Ce6T in films, as observed earlier in related systems[41,42].

The Ce6T molecules in toluene have negligible emission from the S_2 state upon excitation of the Soret band. The fluorescence spectrum is primarily a mirror image of the Q-band, with a maximum at 674 nm and a broad tail (Fig. 1C, dotted curve), as reported[34]. The emission bands have similar decay characteristics (Supplementary Fig. 3A, B) and lifetime (5 ns), confirming their identical origin. In contrast, the thin film emission peak is at 740 nm, and its intensity is four times larger than the band at 674 nm (Fig. 1C, solid curve). Unlike in solution, the two emission bands differed in their decay rate and characteristics, indicating the difference in their origin. The 674 nm emission band decays immediately with a lifetime of 790 ± 30 ps (Supplementary Fig. 3C), whereas the 740 nm band forms with a mono-exponential rise time of 200 ± 10 ps and decays in 1.1 ± 0.1 ns (Supplementary Fig. 3D). We attribute the sharp 674 nm emission to the Ce6T monomer, as in solution, while the 740 nm emission could be from the newly formed excited state species. The excitation spectrum of the thin film Ce6T (Fig. 1D, solid curve), recorded at the emission tail (770 nm), matched with the thin film absorption, indicating that the electronic excitations responsible for the emission are the same as that of absorption. The vibrationless emission, formation time, and long lifetime compared to the 674 nm band thus suggest that the origin of the 740 nm emission band is from an excimer-like state. We call it excimer-like[37–39] because it shows the emission characteristics of an excimer, while we cannot exclude their ground-state interactions as evidenced by the 727 nm absorption peak. The preorganization and assembly of Ce6T

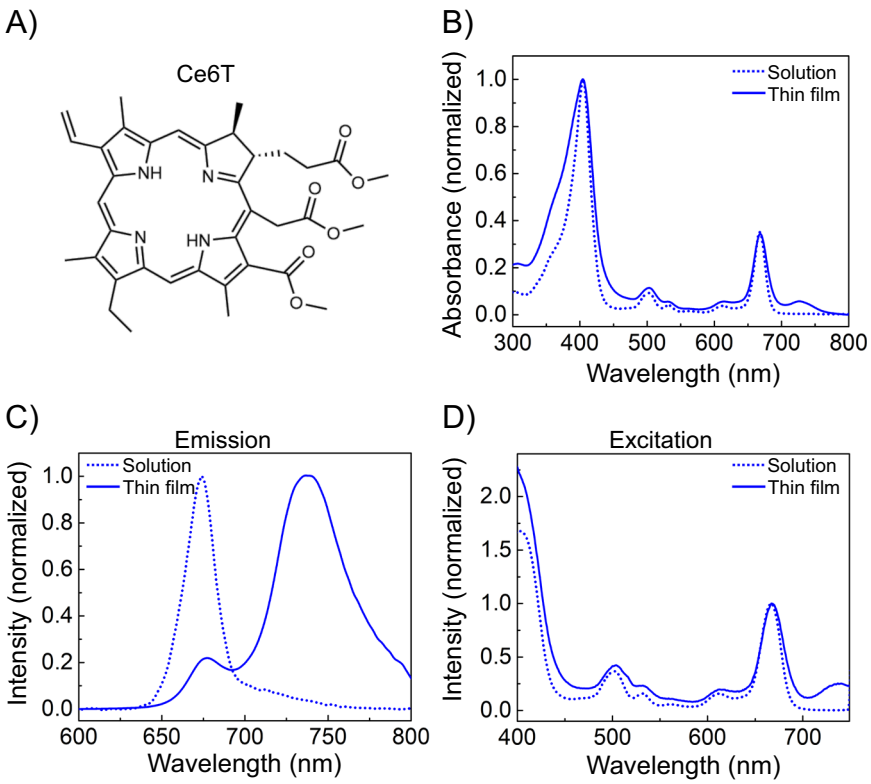

Fig. 1 | Spectroscopic characterization of self-assembled Ce6T. A The schematic illustration of the molecular structure of Ce6T. **B** The absorbance, **C** the emission (λ_{ex} = 450 nm), and (**D**) the excitation (λ_{em} = 770 nm) spectra of Ce6T molecules in toluene (0.01 mM; dotted curve) and in thin films (16 wt% in PS; solid curve).

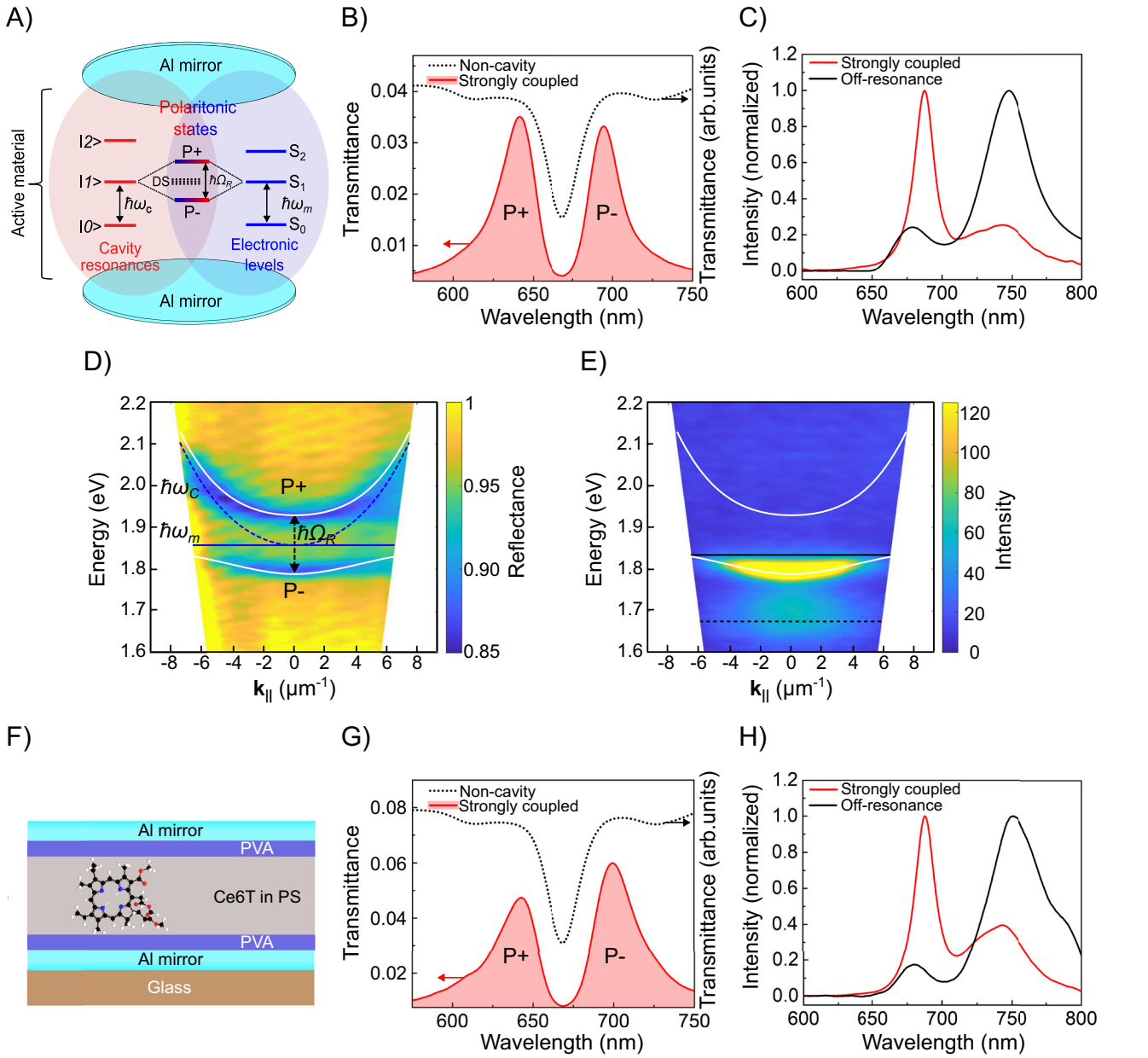

Fig. 2 | Electronic strong coupling of Ce6T Q-band. A The schematic illustration of ESC in an Al/Ce6T/Al Fabry-Perot cavity. **B** The cavity transmittance spectrum shows the splitting of the Ce6T Q-band (black dotted curve) under ESC and the formation of the polaritonic states, P+ and P− (red-shaded curve). **C** The emission spectrum of Ce6T (λ_{ex} = 450 nm) under ESC (red curve) and in an off-resonance cavity (black curve). **D** Angle-resolved white light reflectance plots of strongly coupled Ce6T. The white solid curve shows the coupled oscillator fit of the polaritonic states. The blue dotted curve corresponds to the dispersion of the uncoupled cavity mode ($\hbar\omega_c$), and the blue solid line represents the Ce6T Q-band energy ($\hbar\omega_m$). **E** Angle-resolved emission plot of strongly coupled Ce6T. The white solid curve shows the coupled oscillator fit of the polaritonic states. The black solid and dashed lines show the monomer and the excimer-like emission maxima of the non-cavity Ce6T, respectively. To measure the dispersion, we prepared Fabry-Perot cavities using Ag mirrors. Additional spectral characterization of the Ag cavity is given in Supplementary Fig. 4. **F** Schematic representation of the Al/PVA/Ce6T/PVA/Al cavity. **G** The transmittance spectrum shows the splitting of the Ce6T Q-band (black dotted curve) under ESC and the formation of the polaritonic states (red-shaded curve) in an Al/PVA/Ce6T/PVA/Al cavity. **H** The emission spectra of Ce6T in Al/PVA/Ce6T/PVA/Al cavities under ESC (red curve) and off-resonance (black curve). The λ_{ex} represents the excitation wavelength.

molecules in the thin film results in (i) the coupling of the transition dipoles leading to the 727 nm absorption band and (ii) excimer-like emission upon photoexcitation. Thus, the 727 nm band in the excitation spectrum directly indicates the ground-state intermolecular interactions in Ce6T films.

In ESC experiments, the J-aggregate absorption band is often strongly coupled with the cavity modes[3–9]. Planar molecules, such as porphyrins and phthalocyanines in the absence of bulky substituents, form extended aggregates in thin films, quenching the strong absorption bands of isolated molecules[43]. Then, it is not apparent whether the ESC of the monomer transition will affect the excitonic interactions of the assembled state. In this regard, Ce6T in thin films is different: the absorption characteristics of the isolated molecules are primarily preserved, although a weak exciton coupling band exists due to self-assembly during spin coating. The linear plot of the Q-band absorbance against the varying concentration of Ce6T in the films verifies the above argument (Supplementary Fig. 1C). Thus, Ce6T presents a unique opportunity to probe the ground-state

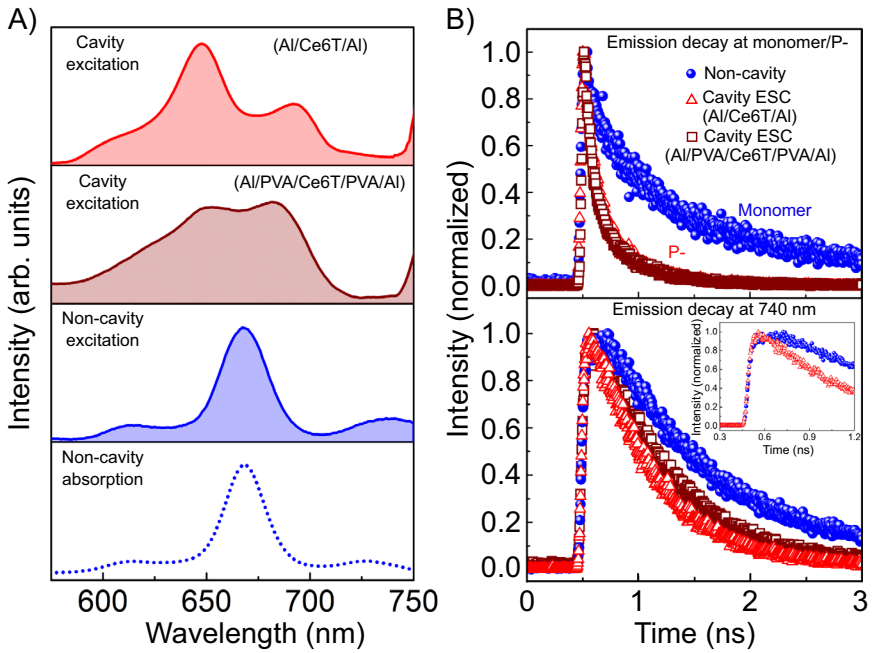

Fig. 3 | Modification of the excitation spectra and emission lifetime of Ce6T under ESC. A The excitation spectrum of Ce6T under ESC in the Al/Ce6T/Al cavity (red shaded curve) and in the Al/PVA/Ce6T/PVA/Al cavity (brown shaded curve). The bottom two panels show the excitation spectrum of non-cavity Ce6T (blue-shaded curve) compared to its absorption spectrum (blue-dotted curve). The excitation spectra were recorded following the emission at 770 nm. **B** The emission decay profile of the non-cavity Ce6T (blue spheres) and strongly coupled Ce6T in the Al/Ce6T/Al cavity (red open triangles) and in the Al/PVA/Ce6T/PVA/Al cavity (brown open squares). The top panel represents the emission decay collected at 674 nm (non-cavity) and 690 nm (under ESC). The bottom panel corresponds to the emission decay collected at 740 nm. The inset in the bottom panel is the zoom of the decay profile, showing the presence and absence of rise time in non-cavity and under ESC, respectively.

intermolecular interactions of the assembled state under the ESC of its Q- and the Soret bands. While the chlorin family of molecules has been the subject of ESC experiments in thin film[44,45] and nanofluidic cavity[46], features corresponding to excitonic interactions were not observed, highlighting the importance of our molecule selection for the present study.

Electronic strong coupling of the Ce6T Q-band

To explore the role of cavity ESC on the intermolecular interaction and the emission from the excimer-like state, we strongly coupled the intense Q-band of Ce6T (λ_{max} = 668 nm; 1.85 eV) by placing spin-coated Ce6T films in a Fabry-Perot cavity made of Al or Ag mirrors of 25 nm thickness (see scheme in Fig. 2A). The concentration of the Ce6T (16 wt% in PS) and film thickness (~400 nm) were optimized to strongly couple the Q-band with the second (λ) mode of the cavity. See Supplementary Discussion. The two new peaks in the transmission spectrum at 642 nm (1.93 eV) and 696 nm (1.78 eV), corresponding to the polaritonic states (P+ and P−), indicate the ESC of the Ce6T Q-band (Fig. 2B, red-shaded curve). The angle-resolved reflectivity plot in Fig. 2D shows the dispersion and the characteristic avoided crossing of the polaritonic states. Further, we extracted the Rabi splitting energy ($\hbar\Omega_R$) from the experimental dispersion curves by fitting it using a simple coupled oscillator model[47,48]. The estimated $\hbar\Omega_R$ from the coupled oscillator model (150 meV) matched well with the transmission (150 meV) and the reflectivity (150 meV) data. The dispersion features of the polaritonic states and the larger $\hbar\Omega_R$ (150 meV) than the FWHM of the cavity mode (120 ± 5 meV) and the Q-band (60 meV) confirm the ESC of the Ce6T Q-band.

We then analyzed the emission properties of the strongly coupled Ce6T by exciting it at 450 nm. The Ce6T under ESC (Fig. 2C red curve) shows an intense narrow emission (λ_{max} = 690 nm) and a weak emission band (λ_{max} = 740 nm). The intense emission band disperses with varying angles of incidence, indicating its polaritonic nature (Fig. 2E, Supplementary Fig. 4). We attribute its origin to the emission from the P- state. The emission dispersion is comparable to that observed for strongly coupled chlorin e6 molecules in nanofluidic cavities[46]. The slight blue shift of the P- emission compared to the absorption has been a feature in many experiments[46,49–51]. The emission from the P+ state is rarely observed in molecular strong coupling at room temperature due to the non-radiative decay to the lower energy levels[46,49–54]. Interestingly, the weak emission (Fig. 2E, Supplementary Fig. 4) showed no dispersive characteristics, indicating a non-polaritonic nature[55,56]. In the off-resonance (Fig. 2C, black curve), red-detuned, and one-mirror cavities (Supplementary Figs. 5–7), the emission spectra resemble the one in non-cavity, confirming that the emission modification originates from the ESC of Q-bands.

To check whether the metal molecule interaction at the mirror-dielectric interface influences the emission features, we prepared cavities by including a poly (vinyl alcohol) (PVA) spacer, as schematically shown in Fig. 2F. We spin-cast the PVA layer (c.a. 15 nm) on top of the bottom Al and separated it from the Ce6T-PS matrix. Similarly, another layer of PVA (c.a. 15 nm) was deposited on top of the Ce6T-PS film to prevent direct contact between the top Al and the Ce6T. We maintained the cavity path length the same as earlier (400 nm) and strongly coupled the Ce6T Q-band to the second mode of the cavity. The observed Rabi splitting (Fig. 2G red shaded curve) in this Al/PVA/Ce6T/PVA/Al cavity is 158 meV and larger than the uncoupled cavity mode width (120 ± 5 meV) and the Ce6T Q-band (60 meV), ensuring the ESC. The emission characteristics (Fig. 2H) of the strongly coupled cavity with a PVA spacer are similar to those of the spacerless (Al/Ce6T/Al) cavities. Again, the off-resonance Al/PVA/Ce6T/PVA/Al cavity emission was similar to that of the non-cavity (Supplementary Fig. 8C). These experiments confirm that the observed changes in emission are due to ESC and not due to any metal-Ce6T interactions.

Interestingly, we do not observe any apparent uncoupled molecular emission in the monomer emission (674 nm) region in the

https://doi.org/10.1038/s41467-025-60025-8

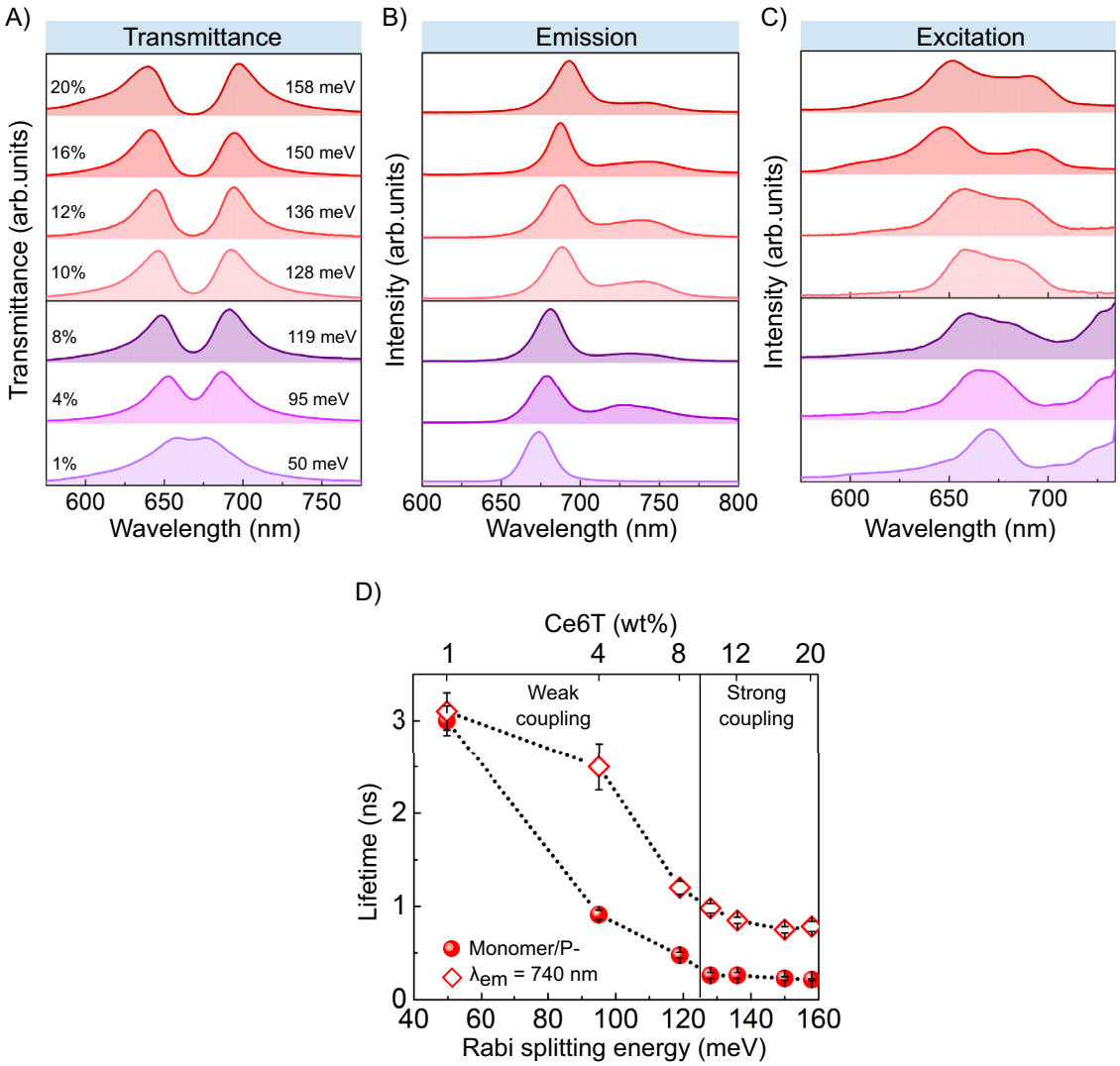

Fig. 4 | Photophysics of Ce6T under weak and strong coupling regimes. A The transmission spectra show changes in the Rabi splitting energy as a function of Ce6T concentration (wt% of Ce6T in PS indicated in the figure). Changes in **B** the emission (λ_{ex} = 450 nm) and (**C**) the excitation (λ_{em} = 770 nm) spectra of Ce6T under weak and strong coupling of the Q-band. The violet- and the red-shaded curves correspond to the weak and strong coupling regimes, respectively. **D** The emission lifetime of Ce6T under weak and strong coupling. The red spheres show the lifetime of the cavity monomer-like emission (P- state under ESC), and the red open diamonds represent the lifetime of the 740 nm band. The error bars correspond to the standard deviation calculated from a minimum of three samples.

strongly coupled cavities. The field amplitude for a second-mode cavity near the metal surface will be higher than a first-mode cavity, and the maximum will be at 1/4th the total path length from either side of the metal, with a node at half the cavity path length[53]. Since the Ce6T molecules are spread across the cavity path length, except for the ~15 nm at the metal interface in Al/PVA/Ce6T/PVA/Al cavities, it is possible to have a fraction of uncoupled molecules emitting at the respective non-cavity Ce6T emission regions. The intensity of the 674 nm emission in the non-cavity itself is low, so the emission from the fraction of uncoupled molecules could be negligible compared to the polaritonic emission. We also notice that, unlike the J-aggregates under ESC[24,49,53,57], the emission spectrum of strongly coupled molecules such as chlorin e6[46], BDAB[51], and fluorescein[51] does not show traces of uncoupled molecule emission. Meanwhile, the weak 740 nm emission observed under ESC in the present case could be thought of as originating from the fraction of uncoupled molecules in a first assumption.

To understand the origin of the weak 740 nm emission band under ESC, we recorded the excitation spectrum by collecting the emission at 770 nm. The excitation spectrum in the top panel of Fig. 3A corresponds to the strongly coupled Ce6T in the Al/Ce6T/Al cavity. The spectrum exhibited peaks at P+ (648 nm) and P− (686 nm) positions and a weak transition at 612 nm, indicating that the non-dispersive, weak emission band (λ_{max} = 740 nm) originates from the excitation of the polaritonic states. The contribution of the P+ state to the emission is relatively more significant than P−, as seen earlier in other experiments[49,51], and suggests that excitation of the two polaritonic states can contribute differently to the observed emission. The surprising and remarkable feature of the excitation spectrum under ESC is the absence of the excitonic coupling peak at 727 nm, in contrast to the absorption and excitation spectra of the non-cavity Ce6T (Fig. 3A, blue dotted and shaded curve). The absence of the 727 nm peak cannot be due to any instrumental limitation when measuring the cavity, as we see the contribution of the weak 612 nm band towards the 740 nm emission, and it also rules out the possibility of a cavity filter effect.

The excitation spectra of the strongly coupled Al/PVA/Ce6T/PVA/Al cavity also showed peaks at P+ and P− positions and the remarkable absence of the excitonic coupling band. Preparation of the Al/PVA/Ce6T/PVA/Al cavities is challenging as there are hydrophilic-

https://doi.org/10.1038/s41467-025-60025-8

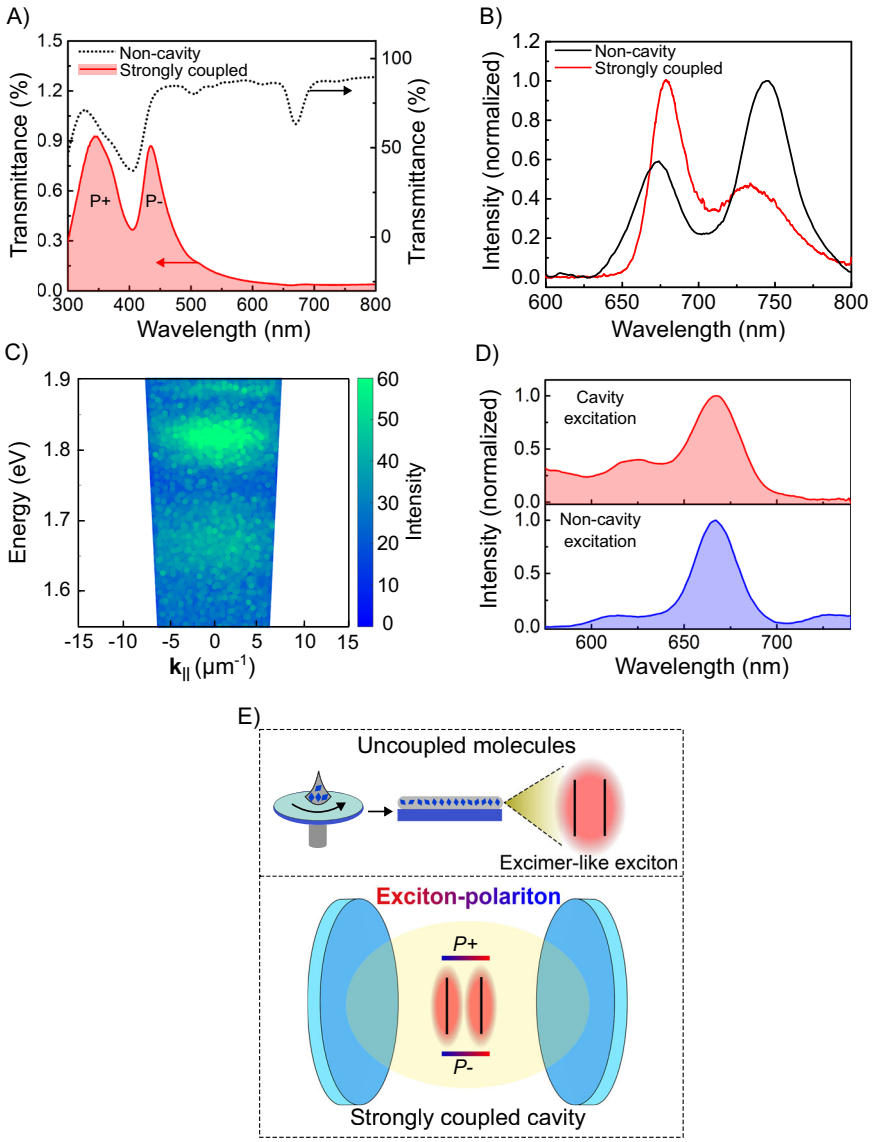

Fig. 5 | Modification of the Ce6T emission properties under the ESC of its Soret band. A The cavity transmittance spectrum (red-shaded curve) shows the splitting of the Ce6T Soret band (black dotted curve) and the formation of the polaritonic states under ESC. **B** The emission spectrum of Ce6T under the ESC of the Soret band (red curve) and in a non-cavity (black curve). The Ce6T-PS film thickness is c.a. 100 nm for the ESC and non-cavity samples, and the excitation wavelength is 440 nm. **C** The angle-resolved emission plot of Ce6T under the ESC of the Soret band shows the non-dispersive emission and the absence of polaritonic character. To measure the dispersion, we prepared Fabry-Perot cavities using Ag mirrors. **D** The excitation spectra of the Soret band strongly coupled Ce6T (red-shaded curve) and the non-cavity Ce6T (blue-shaded curve). We recorded the excitation spectra following the emission at 770 nm. **E** Schematic illustration of the excimer-like exciton formed between two interacting Ce6T molecules in a non-cavity film upon spin coating (top panel). The bottom panel shows the Ce6T molecules with suppressed intermolecular interaction under ESC.

hydrophobic polymer interfaces. It sometimes leads to cavities with broader modes (FWHM = 180 ± 20 meV) than the typical width of Al/Ce6T/Al cavity modes (120 ± 5 meV). Even though former cavities exhibit large splitting (-160 meV) as if under strong coupling, the energy is smaller than the cavity mode width, hence not under ESC. The excitation spectra of such cavities (Supplementary Fig. 8) match the non-cavity, further confirming that the changes to the excitation spectral character only happen under ESC of the Q-band of Ce6T. These observations again prove that we are not observing any filter effects or multiplication of bare molecule absorption and cavity transmission[58] in the excitation spectra. The excitation spectra of off-resonance, far-red detuned, and one-mirror cavities were similar to those of non-cavity (Supplementary Figs. 5–7). Hence, we confirm that the observed changes in the excitation spectra originate from the ESC of the Q-band of Ce6T. Since the 727 nm band is characteristic of the excitonic interaction, its absence in the excitation spectrum suggests that the intermolecular interaction is absent under ESC, despite the assembly of the molecules in the spin-cast film. In other words, the weak, non-dispersive 740 nm emission under ESC differs from the excimer-like emission of non-cavity.

In Fig. 3B, we show the decay of the polaritonic and weak emission bands of both Al/Ce6T/Al (red open triangles) and Al/PVA/Ce6T/PVA/Al cavities (brown open squares) and compare them with non-cavity (blue spheres). The emission decay was analyzed using the time-correlated single photon counting (TCSPC) technique. The P- emission decays nearly three times faster (220 ± 20 ps) than the monomer emission of non-cavity Ce6T (790 ± 30 ps; Fig. 3B top panel). Thus, ESC creates an efficient pathway for the Ce6T molecules to emit through the polaritonic state. The 740 nm band under ESC has a shorter lifetime (800 ± 50 ps) and does not show the rise time compared to the

non-cavity excimer-like emission (bottom panel inset in Fig. 3B). Since an excimer is associated with a rise time[59], the absence of the formation time under ESC indicates that the hybrid-light matter states suppress the transition dipole interactions between Ce6T, preventing excimer-like formation in the thin film. It further signifies that the character of the 740 nm band under ESC differs from the non-cavity excimer-like emission and is closer to the non-cavity monomer. It also indicates that the fraction of uncoupled molecules or their contribution to the emission is negligible in the strongly coupled samples. Once again, the emission decay of the off-resonance, red-detuned, and the one-mirror cavities was identical to that of non-cavity Ce6T molecules (Supplementary Figs. 5–7), and the 740 nm emission under ESC originates from a monomer-like excited state.

Comparison between weak and strong coupling

The weak coupling of light and matter can also modulate the emission properties. However, the weak light-matter coupling typically modifies the radiative decay and is not known to affect other molecular properties[60]. To check the effects of weak and strong coupling, we varied the coupling strength by varying the concentration of the Ce6T molecules, as the Rabi splitting energy varies with the square root of the number of coupled molecules[4]. Since the Al/Ce6T/Al cavities showed the same characteristics under ESC as that of Al/PVA/Ce6T/PVA/Al, and the fabrication of the latter was challenging, we prepared Al/Ce6T/Al cavities for the comparison between weak and strong coupling. We varied the Ce6T concentration from 1 wt% to 20 wt% while maintaining the cavity path length as 400 nm. We recall that the molar extinction coefficient of non-cavity Ce6T did not vary in the concentration range of 1 wt% to 20 wt% (Supplementary Fig. 1C). The Rabi splitting energy observed for 10 wt% of Ce6T (128 ± 5 meV), which is larger than the FWHM of the cavity mode (120 ± 5 meV) and the Ce6T Q-band (60 meV), marks the onset of ESC in our experiments. The red-shaded curves in Fig. 4A show the ESC regime, where the Ce6T concentration is ≥10 wt%. For other lower Ce6T concentrations (Fig. 4A, violet shaded curves), the splitting is less than the FWHM of the cavity modes (120 ± 5 meV) and is in a weak coupling regime. The plot of the Rabi splitting energy against the square root of Ce6T concentration also shows a distinct variation of slopes below and above 10 wt% of Ce6T, indicating a transition from weak to strong light-matter coupling (Supplementary Fig. 9).

Interestingly, the monomer/polaritonic emission is more intense than the 740 nm emission band in both weak and strong coupling regimes (Fig. 4B). The cavity mode in the weak coupling regime almost resonates with the Ce6T emission as the Stokes shift is only 6 nm. Hence, the Purcell effect can enhance the monomer emission under weak coupling[46]. However, for 1 and 4 wt% Ce6T, the weak coupling has less significance as the monomer emission dominates the excimer-like even in non-cavity (Supplementary Fig. 10). In the ESC regime, the P- emission peaks are ≥690 nm, which is 16 nm redshifted compared to the monomer emission band. Therefore, the intense polaritonic emission is not just due to modifying the radiation mode density at the emission wavelength. The excitation spectral response collected at 770 nm, far from the P- emission peak or cavity modes, conspicuously distinguishes the effect of weak and strong coupling on Ce6T films. In the weak coupling regime (Fig. 4C, violet shaded curves), the excitation spectra consist of Q-bands and the excitonic coupling band at 727 nm, as in non-cavity (Supplementary Fig. 10), and the primary excitation responsible for the emission at 770 nm is the 668 nm Q-band. These observations confirm that the weak coupling enhances the emission at the monomeric region without affecting the intermolecular excitonic interaction. Remarkably, under the ESC regime, the primary excitation is through the polaritonic bands, and more interestingly, the 727 nm excitonic coupling band is absent (Fig. 4C, red-shaded curves).

We then analyzed the emission decay in the weak and strong coupling regime and compared it with the non-cavity. The emission lifetime of the monomer and the excimer-like emission decreased steadily in the weak coupling regime (Fig. 4D, red spheres and open diamonds) and in non-cavity (Supplementary Fig. 12), indicative of the enhanced intermolecular interaction with the increase in the concentration of Ce6T. In contrast, under ESC, the lifetime of the polaritonic state (220 ± 20 ps) and the 740 nm band (850 ± 70 ps) remained nearly the same (Fig. 4D and Supplementary Fig. 13). The other remarkable aspect is the presence (weak coupling) and the absence (under ESC) of rise time in the emission decay of the 740 band, showing its distinct character in the weak and strong light-matter coupling regimes.

Photophysics of Ce6T under the ESC of Soret band

Ce6T possesses a strong absorption transition from S_0 to S_2 state, often known as the Soret band. The Soret and the Q-band share the same electronic ground state. Therefore, the ESC of the Soret band could also quench the ground-state excitonic interaction in Ce6T films. To check the latter, we strongly coupled the Ce6T Soret band with the λ/2 (first) cavity mode, whose path length is ~100 nm. A 100 nm thick Ce6T non-cavity film (25% by wt. in PS) showed an OD of 0.5 at 405 nm (Fig. 5A and Supplementary Fig. 14). It maintained all the characteristic features, including the excitonic coupling band at 727 nm, similar to the 400 nm film. The intense excimer-like emission band (Fig. 5B, black curve) and the presence of the 727 nm peak in the excitation spectrum (Fig. 5D, blue shaded curve) confirmed the presence of the excitonic interactions in the Ce6T non-cavity film. Under strong coupling conditions, the Soret band splits to form the polaritonic peaks at 360 nm (P+) and 435 nm (P−), and the large Rabi splitting energy (600 meV) ensures the ESC (cavity mode FWHM = 520 meV, Soret band FWHM = 445 meV).

The emission spectrum of the Soret band strongly coupled Ce6T (Fig. 5B, red curve) showed an intense peak at 679 nm and a less prominent band near the excimer-like emission region. The modified emission of strongly coupled Ce6T compared to the non-cavity (Fig. 5B, black curve) indicates that the ESC of the Soret band and the Q-band of Ce6T impact the photophysics similarly. The transmission spectrum of the Soret band coupled cavity (Fig. 5A, red shaded curve) shows the absence of cavity modes in the emission region of Ce6T that can provide a Purcell enhancement or even act as a filter. Thus, the enhanced emission at the monomeric region offers unequivocal evidence for suppressing the excimer-like state under ESC, which otherwise exists in Ce6T non-cavity of similar thickness. We did not observe considerable emission from the Soret band under ESC conditions, suggesting a faster non-radiative transfer to the emissive Q-bands[61]. The emission bands are non-dispersive (Fig. 5C), indicating the non-polaritonic character. Interestingly, the excitation spectrum of the Soret band coupled Ce6T, recorded by collecting the emission at 770 nm, showed no trace of the excitonic coupling band (Fig. 5D, red shaded curve) contrasting the non-cavity Ce6T (Fig. 5D, blue shaded curve), again pointing to the suppressed intermolecular interaction under ESC. The peaks in the P+ and the P− regions were visible in the excitation spectrum when we collected the emission at 670 nm, which facilitated the excitation from 360 nm (Supplementary Fig. 11B). Additionally, we have analyzed 3λ/2 mode cavities strongly coupled to the Soret band of Ce6T (Supplementary Fig. 14). The results were identical to those of the ESC with the λ/2 mode cavity and showed that the effect of ESC on the assembly of Ce6T is cavity mode independent.

Discussion

Our experiments reveal remarkable features of strongly coupled Ce6T: (i) the modification of emission characteristics, (ii) the absence of the 727 nm excitonic coupling band, and (iii) the nearly constant emission lifetime. We show that although both weak and strong coupling changes the emission characteristics, the underlying mechanism of action is distinctly different. The collective strong coupling suppresses the ground-state excitonic interaction of Ce6T molecules, which

otherwise exist in the preorganized thin film. It leads to the subsequent quenching of an excimer-like state as schematically shown in Fig. 5E. The enhanced monomer-like emission under the ESC of the Ce6T Soret band in a λ/2 cavity is direct evidence for the latter. However, it is difficult to dissect the contribution of the Purcell factor in enhancing the emission under the ESC of the Q-band. The invariant lifetime of polaritonic emission in the ESC regime suggests that the onset of ESC modifies the emission characteristics by establishing newer, or modifying the existing, intermolecular interaction factors. Our observation aligns with recent theoretical studies[25,27], which show that the competition between short-range intermolecular forces and photonic correlation under collective strong coupling induces local changes to the transition density and polarizability of the solvation shell. Interestingly, chlorin e6 (Ce6), a nearly identical molecule to Ce6T, also showed the excitonic coupling band and subsequent excimer-like emission (Supplementary Fig. 15). Remarkably, the strong coupling of the Q-band transition of Ce6 resulted in the suppression of the excimer-like emission, showing that the effect of ESC on intermolecular interactions could hold for different chlorin molecules of similar structures.

The nature of the 740 nm emission under the ESC of Ce6T Q-band is intriguing. The non-dispersive character shows the non-polaritonic nature of the emission[26]. The different lifetimes of the P− and 740 nm emissions suggest they originate from distinct emissive states. A possibility is that the 740 nm emission arises from the excimer-like state in accordance with the 727 nm absorption. Then, there can be fractional population transfer from P+ to P− and subsequently to the lower-lying emissive state. The excitation spectrum under ESC shows the presence of P+ and P− bands. However, the excitonic coupling band at 727 nm is absent, indicating that the excimer-like state is not responsible for the emission at 740 nm. The absence of a rise time signifies that the emission is not from the uncoupled molecules like in a non-cavity, which involves a formation time of 200 ps. The other plausible origin for the 740 nm emission under ESC is from the monomer-like dark states[26]. These dark states are not uncoupled molecules, but collective states generated under strong coupling[4]. Spectroscopically, the dark state levels should be between the polaritonic state energy levels. However, Scholes et al.[26] show that the polaritonic states occupy above the dark states in terms of free energy due to the lower entropy of the former than the latter. It can allow the population to transfer from the polaritonic states to the dark state, from which it can emit[26]. This scenario correlates well with the non-dispersive character of the 740 nm emission, the excitation spectrum, and the absence of rise time under ESC. Therefore, the 740 nm emission band under ESC of the Ce6T Q-band could be from monomer-like dark states, which get populated through the polaritonic states. Thus, ESC suppresses the excimer-like formation in Ce6T and Ce6, and the non-radiative channeling of the excitation energy from the polaritonic states to the emissive molecular states results in the non-dispersive monomer-like emission.

Interestingly, the experiments under VSC have also shown the modification of the dispersion forces[32], crystallization[28], and molecular self-assembly[29–31]. Together with the VSC studies[28–33], our finding that the ESC can change the ground-state intermolecular interactions points to the possibility that collective light-matter strong coupling can alter the weak intermolecular interaction forces, and we argue that the mode of action under VSC or ESC can be similar. Such modifications to the inter- or intra-molecular interactions can indeed cause changes to the phase transition[62] and may open up new conducting pathways[63–66].

Methods

Cavity preparation

The polystyrene (PS, Mw = 192,000), poly(methyl methacrylate) (PMMA, Mw = 120,000), poly (vinyl alcohol) (PVA, Mw = 89,000) were purchased from Merck and used without further purification. Spectroscopy grade toluene was purchased from Sisco Research Laboratories (SRL), Hyderabad, India. Glass slides from CORNING were cut into small pieces (1.5 cm × 1.5 cm), flushed with N_2 gas, and rinsed with milli-Q water to remove dust particles. Subsequently, we cleaned it using ultrasound cleaner (Elma; frequency 35 kHz) in a weakly alkaline solution (0.5% Hellmanex in water), milli-Q water, and ethanol to get a clean impurity-free surface and dried it in a hot air oven at 120 °C. We used a benchtop sputtering tool (HHV Bangalore make, 90 W power, 150 mA current) to deposit the Al mirrors (25 nm thickness) on the dried glass slides. We prepared the solution for spin coating the active material by mixing 10 mg of Ce6T in 4 wt% PS solution (in 1.5 mL toluene) to obtain a 16 wt% Ce6T. Subsequently, we spin-coated the Ce6T-PS solution to get a ~400 nm film on top of the Al or Ag-coated glass slides using PLOS spincoater, Netherlands. The cavities were completed by depositing the top metal layer (25 nm) above the spin-coated Ce6T or Ce6 films. Further, we varied the film thickness to achieve off-resonance and detuned cavities.

Absorption and emission spectra of cavities

The absorbance and transmission of the samples were measured using a Shimadzu UV-Vis 2600 spectrophotometer in the range of 300−800 nm. We recorded the emission and excitation spectra in front-face geometry using a Horiba Jobin Yvon-Spex Fluorolog-3 spectrofluorometer. Reflection and TM polarized emission dispersion measurements of the strongly coupled cavities were performed from −53 ° to +53 ° using a halogen lamp connected to an Eclipse Ti2 (Nikon) inverted microscope[67]. The reflected light was collected through a 100× objective going through a Fourier lens to a spectrometer (SpectraPro HRS-300, Princeton Instruments) coupled to a liquid nitrogen-cooled charge-coupled device (CCD) camera (Pylon 100B×) for spectral acquisition.

Time-resolved emission measurements

We performed the time-correlated single photon counting (TCSPC) measurements in our home-built spectrometer. A BBO crystal is pumped at 900 nm (with 100 fs pulse width and 80 MHz repetition rate, Ti-Sapphire Laser, Mai tai HP) to generate a second harmonic at 450 nm, which we have used for excitation. The excitation laser is focused on the sample using a 10× long working distance objective (with a numerical aperture of 0.26, Mitutoyo Plan Apo NIR Infinity Corrected Objective) to a spot of 2.1 µm diameter. The emission is collected through the same objective, led to the Andor Kymera 328i spectrometer, dispersed by a 300 lines/mm grating, and detected using iDus 416 CCD. For TCSPC, the emission is passed through the spectrometer (used as a monochromator to allow only a specific emission wavelength) and focused on a single-photon avalanche diode (Micro Photon Devices) equipped with a PicoHarp 300 (PicoQuant) timing module. We have used a trigger diode (TDA 200, PicoQuant) to generate the sync signal for the timing module.

The solution state fluorescence lifetimes were recorded with a Horiba Jobin Yvon-IBH make TCSPC system. We excited the sample using a 452 nm pulsed diode laser (NanoLED-450L; 1.2 ns pulse width, repetition rate: 1 MHz) and detected the emission using a microchannel plate detector. The IRF for this setup was 500 ps. The decay curves were fitted using the IBH DAS6.3 software to determine the fluorescence lifetime. The goodness of the fit was determined by a chi-square value less than 1.1 and a standard deviation below ±2.

Coupled oscillator fit

The interaction of the Q-band transition of the chlorin molecule with the λ mode of the Fabry-Perot cavity can be understood by the simple coupled oscillator model[47,48]. Hamiltonian for a strong-coupling interaction can be given as

$$H = \begin{pmatrix} E_x - i\hbar\tau_x & g \\ g & E_c - i\hbar\tau_c \end{pmatrix} \quad (1)$$

Where the E_x is the energy of Q-band transition (1.85 eV), $\hbar\tau_x$ and $\hbar\tau_c$ are the homogenous linewidth of the Q-band and the cavity, respectively. g corresponds to the interaction of the electronic transition with the cavity mode at the resonance condition. The energy of the cavity is dispersive and is dependent on the background refractive index (n_{eff}) as

$$E_c(\theta) = E_0(1 - (\sin\theta/n_{eff})^2)^{-1/2} \quad (2)$$

E_0 is the energy of the cavity and $n_{eff} = 1.58$ for the polystyrene matrix in TM polarization[68].

Data availability

The authors declare that data supporting the findings of this study are available within the paper and its supplementary information files. Source data are provided with this paper.

References

1. Haroche, S. & Kleppner, D. Cavity quantum electrodynamics. *Phys. Today* **42**, 24 (1989).
2. Milonni, P. W. Why spontaneous emission? *Am. J. Phys.* **52**, 340–343 (1984).
3. Genet, C., Faist, J. & Ebbesen, T. W. Inducing new material properties with hybrid light–matter states. *Phys. Today* **74**, 42–48 (2021).
4. Garcia-Vidal, F. J., Ciuti, C. & Ebbesen, T. W. Manipulating matter by strong coupling to vacuum fields. *Science* **373**, eabd0336 (2021).
5. Scholes, G. D. Emergence of collective coherent states from strong-light coupling of disordered systems. *J. Phys. Chem. A* **125**, 6739–6750 (2021).
6. Dovzhenko, D. S., Ryabchuk, S. V., Rakovich, Y. P. & Nabiev, I. R. Light–matter interaction in the strong coupling regime: configurations, conditions, and applications. *Nanoscale* **10**, 3589–3605 (2018).
7. Bhuyan, R. et al. The rise and current status of polaritonic photochemistry and photophysics. *Chem. Rev.* **123**, 10877–10919 (2023).
8. Hirai, K., Hutchison, J. A. & Uji-i, H. Molecular chemistry in cavity strong coupling. *Chem. Rev.* **123**, 8099–8126 (2023).
9. Tibben, D. J. et al. Molecular energy transfer under the strong light–matter interaction regime. *Chem. Rev.* **123**, 8044–8068 (2023).
10. Purcell, E. M. Spontaneous emission probabilities at radio frequencies. in: Burstein, E. & Weisbuch, C. (eds) *Confined Electrons and Photons: New Physics and Applications*. 839–839 (Springer US, Boston, MA, 1995).
11. Li, J.-F., Li, C.-Y. & Aroca, R. F. Plasmon-enhanced fluorescence spectroscopy. *Chem. Soc. Rev.* **46**, 3962–3979 (2017).
12. Aslan, K. et al. Metal-enhanced fluorescence: an emerging tool in biotechnology. *Curr. Opin. Biotechnol.* **16**, 55–62 (2005).
13. Hutchison, J. A., Schwartz, T., Genet, C., Devaux, E. & Ebbesen, T. W. Modifying chemical landscapes by coupling to vacuum fields. *Angew. Chem. Int. Ed. Engl.* **51**, 1592–1596 (2012).
14. Mony, J. et al. Photoisomerization efficiency of a solar thermal fuel in the strong coupling regime. *Adv. Funct. Mater.* **31**, 2010737 (2021).
15. Zeng, H. et al. Control of photoswitching kinetics with strong light–matter coupling in a cavity. *J. Am. Chem. Soc.* **145**, 19655–19661 (2023).
16. Lee, I., Melton, S. R., Xu, D. & Delor, M. Controlling molecular photoisomerization in photonic cavities through polariton funneling. *J. Am. Chem. Soc.* **146**, 9544–9553 (2024).
17. Coles, D. M. et al. Polariton-mediated energy transfer between organic dyes in a strongly coupled optical microcavity. *Nat. Mater.* **13**, 712–719 (2014).
18. Zhong, X. et al. Energy transfer between spatially separated entangled molecules. *Angew. Chem. Int. Ed. Engl.* **56**, 9034–9038 (2017).
19. Akulov, K., Bochman, D., Golombek, A. & Schwartz, T. Long-distance resonant energy transfer mediated by hybrid plasmonic–photonic modes. *J. Phys. Chem. C.* **122**, 15853–15860 (2018).
20. Bhatt, P., Dutta, J., Kaur, K. & George, J. Long-range energy transfer in strongly coupled donor–acceptor phototransistors. *Nano Lett.* **23**, 5004–5011 (2023).
21. Munkhbat, B., Wersäll, M., Baranov, D. G., Antosiewicz, T. J. & Shegai, T. Suppression of photo-oxidation of organic chromophores by strong coupling to plasmonic nanoantennas. *Sci. Adv.* **4**, eaas9552 (2018).
22. Peters, V. N. et al. Effect of strong coupling on photodegradation of the semiconducting polymer P3HT. *Optica* **6**, 318–325 (2019).
23. Hutchison, J. A. et al. Tuning the work-function via strong coupling. *Adv. Mater.* **25**, 2481–2485 (2013).
24. Canaguier-Durand, A. et al. Thermodynamics of molecules strongly coupled to the vacuum field. *Angew. Chem. Int. Ed. Engl.* **52**, 10533–10536 (2013).
25. Haugland, T. S., Schäfer, C., Ronca, E., Rubio, A. & Koch, H. Intermolecular interactions in optical cavities: an ab initio QED study. *J. Chem. Phys.* **154**, 094113 (2021).
26. Scholes, G. D., DelPo, C. A. & Kudisch, B. Entropy reorders polariton states. *J. Phys. Chem. Lett.* **11**, 6389–6395 (2020).
27. Castagnola, M., Haugland, T. S., Ronca, E., Koch, H. & Schäfer, C. Collective strong coupling modifies aggregation and solvation. *J. Phys. Chem. Lett.* **15**, 1428–1434 (2024).
28. Hirai, K., Ishikawa, H., Chervy, T., Hutchison, J. A. & Uji-i, H. Selective crystallization via vibrational strong coupling. *Chem. Sci.* **12**, 11986–11994 (2021).
29. Joseph, K. et al. Supramolecular assembly of conjugated polymers under vibrational strong coupling. *Angew. Chem. Int. Ed.* **60**, 19665–19670 (2021).
30. Joseph, K. et al. Consequences of vibrational strong coupling on supramolecular polymerization of porphyrins. *J. Am. Chem. Soc.* **146**, 12130–12137 (2024).
31. Zhong, C. et al. Driving DNA origami coassembling by vibrational strong coupling in the dark. *ACS Photonics* **10**, 1618–1623 (2023).
32. Patrahau, B. et al. Direct observation of polaritonic chemistry by nuclear magnetic resonance spectroscopy. *Angew. Chem. Int. Ed.* **63**, e202401368 (2024).
33. Sandeep, K. et al. Manipulating the self-assembly of phenyleneethynylenes under vibrational strong coupling. *J. Phys. Chem. Lett.* **13**, 1209–1214 (2022).
34. Nagano, Y., Ogasawara, S. & Tamiaki, H. Regioisomeric synthesis of chlorin-e6 dimethyl esters and their optical properties. *J. Porphyr. Phthalocyanines* https://doi.org/10.1142/S1088424618501043 (2018).
35. Balaban, T. S., Tamiaki, H. & Holzwarth, A. R. Chlorins Programmed for Self-Assembly. in: Würthner, F. (ed.) *Supermolecular Dye Chemistry*. 1–38 (Springer, Berlin, Heidelberg, 2005).
36. Tamiaki, H. et al. Synthetic zinc and magnesium chlorin aggregates as models for supramolecular antenna complexes in chlorosomes of green photosynthetic bacteria. *Photochem. Photobiol.* **63**, 92–99 (1996).
37. Winnik, F. M. Photophysics of preassociated pyrenes in aqueous polymer solutions and in other organized media. *Chem. Rev.* **93**, 587–614 (1993).
38. Neuteboom, E. E., Meskers, S. C. J., Meijer, E. W. & Janssen, R. A. J. Photoluminescence of self-organized perylene bisimide polymers. *Macromol. Chem. Phys.* **205**, 217–222 (2004).
39. Giaimo, J. M. et al. Excited singlet states of covalently bound, cofacial dimers and trimers of perylene-3,4:9,10-bis(dicarboximide)s. *J. Phys. Chem. A* **112**, 2322–2330 (2008).
40. Lehn, J.-M. Toward complex matter: supramolecular chemistry and self-organization. *Proc. Natl Acad. Sci. USA* **99**, 4763–4768 (2002).

41. Byrdin, M. et al. Light harvesting in photosystem I: modeling based on the 2.5-Å structure of photosystem I from Synechococcus elongatus. *Biophys. J.* **83**, 433–457 (2002).
42. Wang, X.-F., Kitao, O., Zhou, H., Tamiaki, H. & Sasaki, S. Efficient dye-sensitized solar cell based on oxo-bacteriochlorin sensitizers with broadband absorption capability. *J. Phys. Chem. C.* **113**, 7954–7961 (2009).
43. Würthner, F., Kaiser, T. E. & Saha-Möller, C. R. J-Aggregates: from serendipitous discovery to supramolecular engineering of functional dye materials. *Angew. Chem. Int. Ed. Engl.* **50**, 3376–3410 (2011).
44. Coles, D. M. et al. Strong coupling between chlorosomes of photosynthetic bacteria and a confined optical cavity mode. *Nat. Commun.* **5**, 5561 (2014).
45. Wu, F. et al. Optical cavity-mediated exciton dynamics in photosynthetic light harvesting 2 complexes. *Nat. Commun.* **13**, 6864 (2022).
46. Bahsoun, H. et al. Electronic light–matter strong coupling in nanofluidic Fabry–Pérot cavities. *ACS Photonics* **5**, 225–232 (2018).
47. Bajoni, D. Polariton lasers. Hybrid light–matter lasers without inversion. *J. Phys. Appl. Phys.* **45**, 313001 (2012).
48. Graf, A., Tropf, L., Zakharko, Y., Zaumseil, J. & Gather, M. C. Near-infrared exciton-polaritons in strongly coupled single-walled carbon nanotube microcavities. *Nat. Commun.* **7**, 13078 (2016).
49. Schwartz, T. et al. Polariton dynamics under strong light–molecule coupling. *ChemPhysChem* **14**, 125–131 (2013).
50. Mony, J. et al. Interplay between polaritonic and molecular trap states. *J. Phys. Chem. C.* **126**, 7965–7972 (2022).
51. George, J. et al. Ultra-strong coupling of molecular materials: spectroscopy and dynamics. *Faraday Discuss* **178**, 281–294 (2015).
52. Vasista, A. B., Menghrajani, K. S. & Barnes, W. L. Polariton assisted photoemission from a layered molecular material: role of vibrational states and molecular absorption. *Nanoscale* **13**, 14497–14505 (2021).
53. Wang, S. et al. Quantum yield of polariton emission from hybrid light-matter states. *J. Phys. Chem. Lett.* **5**, 1433–1439 (2014).
54. Kéna-Cohen, S., Maier, S. A. & Bradley, D. D. C. Ultrastrongly coupled exciton–polaritons in metal-clad organic semiconductor microcavities. *Adv. Opt. Mater.* **1**, 827–833 (2013).
55. Stanley, R. P., Houdré, R., Weisbuch, C., Oesterle, U. & Ilegems, M. Cavity-polariton photoluminescence in semiconductor microcavities: experimental evidence. *Phys. Rev. B* **53**, 10995–11007 (1996).
56. Houdré, R. Early stages of continuous wave experiments on cavity-polaritons. *Phys. Status Solidi B* **242**, 2167–2196 (2005).
57. Hobson, P. A. et al. Strong exciton–photon coupling in a low-Q all-metal mirror microcavity. *Appl. Phys. Lett.* **81**, 3519–3521 (2002).
58. Dutta, A. et al. Thermal disorder prevents the suppression of ultrafast photochemistry in the strong light-matter coupling regime. *Nat. Commun.* **15**, 6600 (2024).
59. Pensack, R. D., Ashmore, R. J., Paoletta, A. L. & Scholes, G. D. The nature of excimer formation in crystalline pyrene nanoparticles. *J. Phys. Chem. C.* **122**, 21004–21017 (2018).
60. Aberra Guebrou, S. et al. Coherent emission from a disordered organic semiconductor induced by strong coupling with surface plasmons. *Phys. Rev. Lett.* **108**, 066401 (2012).
61. Holmes, R. J. & Forrest, S. R. Exciton-photon coupling in organic materials with large intersystem crossing rates and strong excited-state molecular relaxation. *Phys. Rev. B* **71**, 235203 (2005).
62. Jarc, G. et al. Cavity-mediated thermal control of metal-to-insulator transition in 1T-TaS2. *Nature* **622**, 487–492 (2023).
63. Orgiu, E. et al. Conductivity in organic semiconductors hybridized with the vacuum field. *Nat. Mater.* **14**, 1123–1129 (2015).
64. Bhatt, P., Kaur, K. & George, J. Enhanced charge transport in two-dimensional materials through light–matter strong coupling. *ACS Nano* **15**, 13616–13622 (2021).
65. Kumar, S. et al. Extraordinary electrical conductance through amorphous nonconducting polymers under vibrational strong coupling. *J. Am. Chem. Soc.* **146**, 18999–19008 (2024).
66. Fukushima, T., Yoshimitsu, S. & Murakoshi, K. Inherent promotion of ionic conductivity via collective vibrational strong coupling of water with the vacuum electromagnetic field. *J. Am. Chem. Soc.* **144**, 12177–12183 (2022).
67. Johns, B., Kaur, K. & George, J. Tailoring the photoluminescence of monolayer WS2 under weak and strong coupling regimes. *ACS Appl. Opt. Mater.* **2**, 2426–2434 (2024).
68. Becker, M. R. et al. Waveguide optical properties of polystyrene doped with *p*-nitroaniline derivatives. *Opt. Mater.* **32**, 1526–1531 (2010).

Acknowledgments

We thank the Department of Inorganic and Physical Chemistry, IISc, Prof. S. Ramakrishnan (IISc Bengaluru), Prof. K. George Thomas (IISER-Thiruvananthapuram), and Prof. Jino George (IISER-Mohali) for providing access to instrumentation facilities. We thank Dr. Jhuma Dutta (IISER-Mohali) and Mr. Livin Paul (IISER-Thiruvananthapuram) for helping us with the measurements. We thank Ms. Rashmita (visiting student from NISER Bhubaneswar) and Ms. Adhwithi P (visiting student from CUSAT, Kerala) for their help with sample preparation. S.B., M.M., and K.S.M. thank the Prime Minister's Research Fellowship (PMRF) for the Ph.D. fellowship. G.C. thanks SERB for the fellowship. A.S. thanks IISc for the start-up grant, Infosys Foundation for the Young Investigator Award, and MoE-STARS (STARS-2/2023-0265) funding. A.T. thanks IISc for the start-up grant (IE/CARE-21-0321 and SR/MHRD-20-0039), DST-SERB for the core research grant (CRG/2021/002396), and Infosys Foundation for Young Investigator Award (FG/OTHR-21-1050). We thank Dr. Thibault Chervy and Dr. Veerbhadrarao Kaliginedi for the helpful discussion.

Author contributions

S.B. conceptualized and designed the experiments; S.B. and G.C. prepared samples and performed the spectroscopic characterization. M.M. performed the time-resolved emission measurements, A.S. supervised the time-resolved emission measurements; K.S.M. and A.T. performed the coupled oscillator fit. A.T. conceived the idea, conceptualized and designed the experiments, and supervised the project. S.B., M.M., G.C., K.S.M., A.S., and A.T. analyzed and discussed all the data. S.B., A.S., and A.T. wrote the manuscript with inputs from all authors.

Competing interests

The authors declare no conflict of interest.

Additional information

Supplementary information The online version contains supplementary material available at https://doi.org/10.1038/s41467-025-60025-8.

Correspondence and requests for materials should be addressed to Akshay Singh or Anoop Thomas.

Peer review information *Nature Communications* thanks the anonymous reviewer(s) for their contribution to the peer review of this work. A peer review file is available.

Reprints and permissions information is available at http://www.nature.com/reprints

Publisher's note Springer Nature remains neutral with regard to jurisdictional claims in published maps and institutional affiliations.

Open Access This article is licensed under a Creative Commons Attribution-NonCommercial-NoDerivatives 4.0 International License, which permits any non-commercial use, sharing, distribution and reproduction in any medium or format, as long as you give appropriate credit to the original author(s) and the source, provide a link to the Creative Commons licence, and indicate if you modified the licensed material. You do not have permission under this licence to share adapted material derived from this article or parts of it. The images or other third party material in this article are included in the article's Creative Commons licence, unless indicated otherwise in a credit line to the material. If material is not included in the article's Creative Commons licence and your intended use is not permitted by statutory regulation or exceeds the permitted use, you will need to obtain permission directly from the copyright holder. To view a copy of this licence, visit http://creativecommons.org/licenses/by-nc-nd/4.0/.

© The Author(s) 2025